Attractor Merging Crisis in the Double–Scroll Oscillator*

B. Reisner, A. Kittel, S. Lück, J. Peinke, and J. Parisi

Physical Institute, University of Bayreuth, D-95440 Bayreuth

Z. Naturforsch. **50 a,** 1105–1107 (1995); received August 16, 1995

We investigate the transition from a mono–scroll to a double–scroll attractor observed in the chaotic dynamics of an electronic oscillator. The description in terms of an attractor merging crisis turns out to be successful. The finding is supported by the topological structure of the attractor and the scaling behavior of the mean residence time.

In a nonlinear system it is often found that a small variation of one control parameter can lead to sudden changes in the extension of its chaotic attractor. Following Grebogi, Ott, and Yorke [1], this phenomenon is called crisis. So far, one distinguishes between an attractor destruction, an attractor widening, and an attractor merging crisis [2]. In all cases, the crisis is a collision between the chaotic attractor and a coexisting unstable periodic orbit or unstable fixed point. The collision is responsible for the change in the shape of the attractor. The value of the control parameter where the crisis occurs is called the critical value. In the following we study the attractor merging crisis. There, the system flips between the two parts of the merged attractor consisting of the formerly separated ones. We characterize this crisis by the average time the system spends on one part of the attractor, the so–called mean residence time. In the vicinity of the critical parameter value, there exists a scaling behavior of the mean residence time that is predicted to follow a power law with a characteristic exponent γ.

We investigate a particular transition in the system dynamics of an autonomous electronic oscillator that has a striking appearance in the bifurcation diagram. Our experiment consists of an electric circuit capable to exhibit chaotic current and voltage oscillations. The circuit sketched in Fig. 1 was introduced by Shinriki et al. [3]. The system variables are V_1 and V_2, the voltages across the capacitors C_1 and C_2, respectively, and I_3, the current through the resistor R_3. The control parameter is the resistance of R_2. The nonlinear

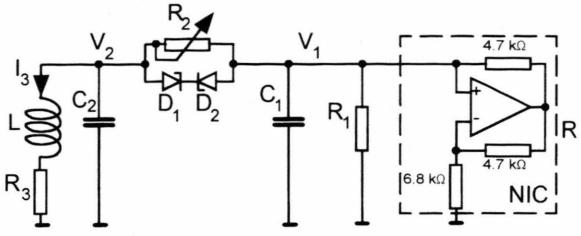

Fig. 1. The scheme of the nonlinear oscillator. The variable resistor R_2 is a precision resistor decade. The operation amplifier is of the type INA 101 biased with $\pm 15\,V$. The diodes D_1 and D_2 are 3.3 V Zener diodes of the type BZX55C 3V3.

element of the circuit is represented by the parallel connection of the two Zener diodes D_1 and D_2 and the resistor R_2. The equations of state are given as:

$$\begin{aligned} C_1\,\dot{V}_1 &= -V_1\left(\frac{1}{R_N}+\frac{1}{R_1}\right) - f\,(V_1 - V_2)\,, \\ C_2\,\dot{V}_2 &= f\,(V_1 - V_2) - I_3, \\ L\,\dot{I}_3 &= -I_3 R_3 + V_2. \end{aligned} \tag{1}$$

The function $f(V_1 - V_2)$ represents the I-V characteristic of the parallel connection of the Zener diodes and the resistor R_2. It shunts the resonant circuit LC_2 with the parallel connection consisting of R_N, R_1, and C_1. Note that R_N possesses a negative value of resistance that is realized by a so–called negative impedance converter (NIC). The latter is marked by a dashed box in Figure 1. It has been constructed on the basis of the operation amplifier INA 101. In our experiment we used the following fixed parameters: C_1 = 10.6 nF, C_2 = 101 nF, L = 323 mH, $R_N = -6.98$ kΩ, R_1 = 21.8 kΩ, R_3 = 99.4 Ω.

* Paper presented at the 5th Annual Meeting of ENDADYN, Grenoble, October 10 - 13, 1994.

Reprint requests to Prof. Dr. J. Parisi.

0932-0784 / 95 / 1200-1105 $ 06.00 © – Verlag der Zeitschrift für Naturforschung, D-72072 Tübingen

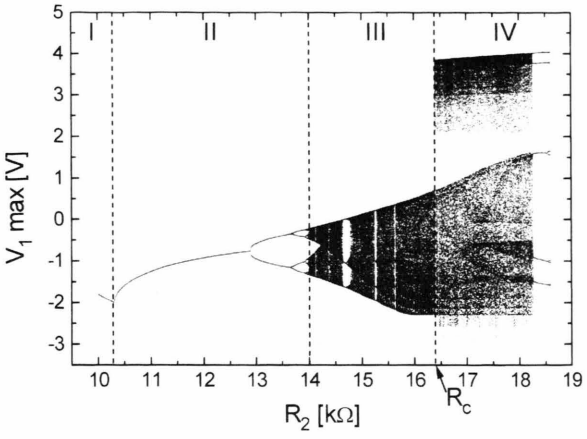

Fig. 2. The experimental bifurcation diagram. The distribution of the maxima of the voltage V_1 is plotted as a function of the control parameter R_2. The distinct regimes are marked as follows: (I) stable fixed point, (II) period–doubling scenario, (III) mono–scroll chaos, and (IV) double–scroll chaos. The critical resistance value R_c is also marked.

Figure 2 shows the measured bifurcation diagram. Upon increasing R_2, the system behavior develops via the following scenario: stable fixed point (I), period–doubling scenario (II), mono–scroll (Rössler type) chaos (III), and double–scroll chaos (IV). We restrict ourselves to the transition from mono–scroll to double–scroll chaos. The corresponding critical value R_c is marked accordingly. For the areas III and IV, the typical experimental phase portraits are displayed in Figure 3. It is easy to see that the structure of the mono–scroll attractor (a) again appears in the double–scroll attractor (b), when the attractor merging crisis has occurred.

In order to inspect the crisis in our electronic oscillator, we consider the mean residence time the system spends in one part of the double–scroll attractor. This part stems from the mono–scroll attractor in the case of the two originally separated attractors. Therefore, we have measured the time series of the three variables V_1, V_2, and I_3. An example of a time series produced by a double–scroll attractor is shown in Figure 4. Obviously, the time series consists of a switching between two levels and an oscillation around each of them. Since the time series of only one single variable does not allow for the discrimination of the two parts of the attractor, we use the time series of all three observables. For the determination of the residence times, a plane which separates the two parts of the attractor in phase space is constructed. The

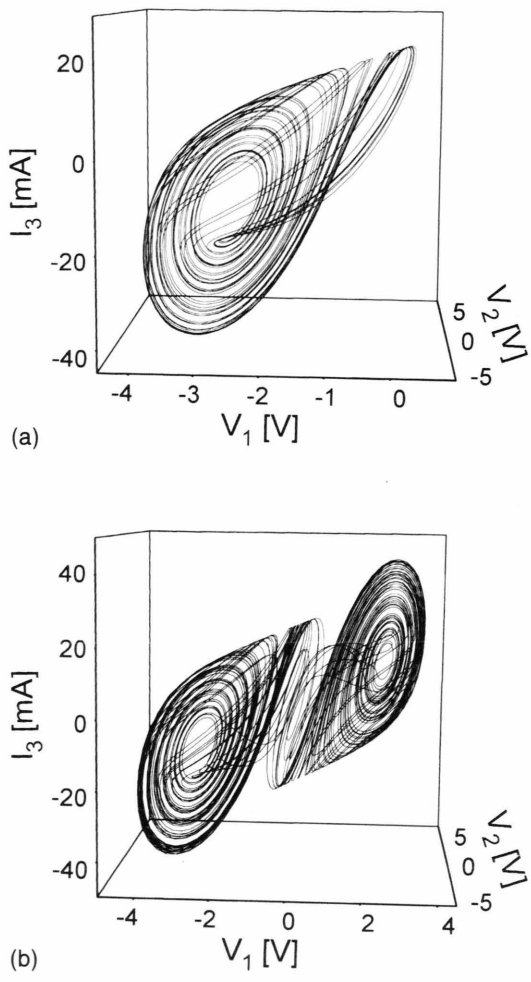

Fig. 3. Typical phase portraits of the experimental system corresponding to different regimes: (a) mono–scroll chaos from region III (R_2 = 15.9 kΩ), (b) double–scroll chaos from region IV (R_2 = 17.0 kΩ).

beginning and the end of the residence time are defined by the times when the trajectory crosses the above plane in either direction. In detail, we calculate the normal component of the trajectory with respect to the plane. The change of the sign of the normal component indicates the transition event. For a reasonable statistical approximation we take the average of about 300 measured values of the residence time. The scaling behavior is analyzed by recording the mean residence time $\langle\tau\rangle$ for different values of the resistance R_2. In Fig. 5(a) the graph $\log\langle\tau\rangle$ vs. $\log(R - R_c)$ is plotted. For a fit of the experimental data, we assume the scaling behavior predicted for an attractor merging crisis. The parameters R_c and

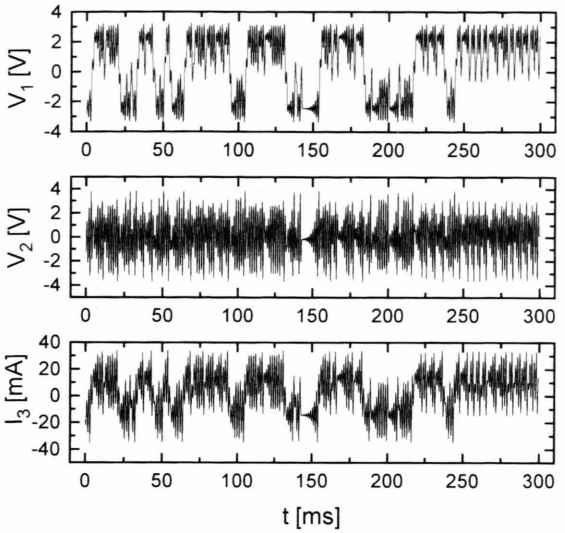

Fig. 4. One typical set of time series of the variables V_1, V_2, and I_3 forming a double–scroll attractor (R_2 = 17.0 kΩ).

γ of the law $\langle\tau\rangle \propto (R - R_c)^\gamma$ [4], were taken as $R_c = (16.40 \pm 0.02)$ kΩ and $\gamma = -0.82 \pm 0.01$. Indeed, we have confirmed this scaling law over one and a half decades. Its validity is limited for values of R close to R_c by the inevitable drift of the system towards the mono–scroll area. In experiment, we therefore start with a value of R_2 above the critical one R_c and decrease R_2 carefully towards that critical value. For values of R far away from R_c (i. e., $(R - R_c) > 1000\Omega$), there exists a periodic window in the double-scroll area, which makes it impossible to verify the scaling law any further. In addition, we would like to point out that far from the critical value R_c the residence time is limited by the characteristic time of the electronic oscillator, $t_0 = 2\pi\sqrt{C_2 L}$.

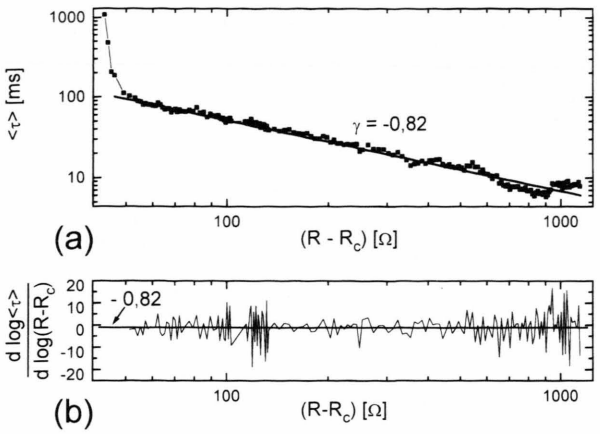

Fig. 5. (a) Double–logarithmic plot of the mean residence time versus the distance of the resistance from the critical value. The slope of the straight line is given by $\gamma = -0.82$. (b) The logarithmic derivation $\mathrm{d}\log\langle\tau\rangle / \mathrm{d}\log(R - R_c)$ shows the scattering around the value $\gamma = -0.82$.

In our case it is t_0 = 1.13 ms. To illustrate the scattering of the measured data around the predicted law, Fig. 5(b) displays the logarithmic derivation $\mathrm{d}\log\langle\tau\rangle / \mathrm{d}\log(R - R_c)$. Here, we can also see that over more than one decade there is hardly any systematic deviation from the observed power law behavior. Obviously, all fluctuations seem to be uniformly distributed around the mean value $\gamma = -0.82$.

To conclude, the transition between the mono–scroll and the double–scroll attractor can be described as an attractor merging crisis with a characteristic scaling of the mean residence time versus the control parameter R_2 governed by the predicted power law $\langle\tau\rangle \propto (R - R_c)^\gamma$ with $\gamma = -0.82$.

The authors would like to thank J. Vollmer and R. Richter for fruitful discussions.

[1] C. Grebogi, E. Ott, and J.A. Yorke, Phys. Rev. Lett. **48**, 1507 (1982).

[2] C. Grebogi, E. Ott, F. Romeiras, and J.A. Yorke, Phys. Rev. A **36**, 5365 (1987).

[3] M. Shinriki, M. Yamamoto, and S. Mori, Proc. IEEE **69**, 394 (1981).

[4] C. Grebogi, E. Ott, and J.A. Yorke, Physica **7D**, 181 (1983).

Sliding Dynamics of the Frenkel-Kontorova Model*

T. Strunz

Institut für Physik, Klingelbergstr. 82, CH-4056 Basel

Z. Naturforsch. **50 a,** 1108–1112 (1995); received August 16, 1995

We investigate the dynamics of the Frenkel-Kontorova model with inertia and damping under a uniform driving force.

We consider the dependence of the velocity-force characteristic, and the corresponding sliding states on the damping: In the overdamped limit the asymptotic solution with nonzero sliding velocity is unique and periodic. Periodic solutions and their stability can also be calculated for decreasing damping, where the dynamics is dominated by resonance effects of the underlying potential with the phonon modes of the chain. The asymptotic velocity is not unique, leading to hysteresis in the velocity-force characteristic. In addition to periodic sliding states, which lose stability for decreasing damping, quasiperiodic or spatio-temporal chaotic behavior occurs.

1. Introduction

The dynamics of a one-dimensional harmonic chain, subject to a periodic potential (Frenkel-Kontorova model [1]) is an example of a dynamical system where many degrees of freedom are essential. Depending on the system parameters and the mode of driving the dynamics of the chain is known to exhibit complex behavior like self-organized criticality [2].

In this work we study the uniformly driven dynamics of the chain which is related to models of sliding friction of clean atomic surfaces [3], to classical models of transport phenomena in charge-density wave (CDW) conductors [4], and to models of Josephson junction arrays [5].

As an extension to other studies we include inertia terms in the equation of motion and investigate the underdamped dynamics.

1.1. Model

The potential energy of the Frenkel-Kontorova model with N particles reads

$$U = \frac{1}{2}\sum_j (x_{j+1} - x_j)^2 - \sum_j b \cos x_j .$$

The mean particle spacing a is enforced by the periodic boundary condition $x_{j+N} = 2\pi L + x_j$, with L an integer so that $a = 2\pi L/N$. We are interested in the limit $N \to \infty$, and especially in the case where the average particle distance is incommensurate with the period of the potential, i.e. L/N approaches an irrational number α. We consider the case where α is the golden mean, i.e. $\alpha = (1+\sqrt{5})/2$, so that L and N are chosen as successive elements of the Fibonacci series.

1.2. Stationary States

The properties of the stationary states, i.e. the solutions of $\partial U/\partial x_j = 0$, have been clarified by Aubry [6]. In the incommensurate case the ground state is described by an analytic hull-function f_S,

$$x_j = ja + \zeta + f_S(ja + \zeta)$$

with $f_S(\xi + 2\pi) = f_S(\xi)$ and ζ arbitrary, if the potential strength b is below a critical value $b_c \approx 0.97\ldots$. Because of the translational invariance of the ground state a Goldstone mode exists. A uniformly applied force F therefor leads to a sliding state, so that no stationary states exist for $F \neq 0$ and $b < b_c$. Above b_c, stationary configurations exist and the ground is again described by a hull-function, now being non-analytic. In this case the chain is pinned, and stationary configurations exist until the force exceeds a critical value $F_c(b)$.

* Paper presented at the 5th Annual Meeting of ENDADYN, Grenoble, October 10 - 13, 1994.

Reprint requests to Dipl. Phys. T. Strunz.

0932-0784 / 95 / 1200-1108 $ 06.00

1.3. Dynamics

The relaxational dynamics of the uniformly driven system

$$\dot{x}_j = -\frac{\partial U}{\partial x_j} + F$$

has been studied by Coppersmith and Fisher [7] in the case where α is the golden mean. It can be shown that in the case of relaxational dynamics the sliding solution is unique [8]. The sliding solution is given by an analytic hull-function f_F:

$$x_j(t) = ja + vt + f_F(ja + vt), \tag{1}$$

where $f_F(\xi + 2\pi) = f_F(\xi)$, and v is the average velocity uniquely determined by F. The particles move periodically. Each particle performs the same motion, only shifted by a certain phase. This holds true for any a. But the critical behavior for $F \to F_c$ depends on whether the chain is commensurate or incommensurate. If the force approaches the critical value from above, the velocity behaves as $v \sim (F - F_c)^\zeta$, with $\zeta = \frac{1}{2}$ in the commensurate case and $\zeta \simeq 0.67$ in the incommensurate case where $F_c \neq 0$, i.e. $b > b_c$.

We now consider the equation of motion with inertia (mass = 1) and damping:

$$\ddot{x}_j = -\gamma \dot{x}_j - 2x_j + x_{j+1} + x_{j-1} - b \sin x_j + F. \tag{2}$$

After a heuristic consideration we discuss periodic solutions of the type (1) for arbitrary values of the damping. We calculate these solutions and their stability numerically. It turns out that periodic solutions are unstable for small values of the damping and the numerical integration of the equations of motion shows more complex sliding states. In addition the sliding state is no longer uniquely determined by the force, which leads to hysteresis. Also the depinning transition becomes subcritical.

2. Sliding Dynamics

2.1. Heuristic Considerations

In order to gain some insight in the sliding solutions of (2) one can assume a solution with mean velocity v in the form

$$x_j(t) = aj + vt + \delta x_j,$$

so that the δx_j are the particle positions in the reference frame of the moving chain. The spatial Fourier transform of the linearized equation of motion in δx reads

$$\begin{aligned}\delta\ddot{x}_k = &-\gamma\delta\dot{x}_k - \omega^2(k)\delta x_k \\ &+ \frac{ib}{2}(e^{ivt}\delta_{k,a} - e^{-ivt}\delta_{k,-a}) \\ &- \frac{b}{2}(e^{ivt}\delta x_{k-a} + e^{-ivt}\delta x_{k+a}) \\ &+ (F - \gamma v)\delta_{k,0}.\end{aligned}$$

Here $k \in [-\pi, \pi]$, a is the average particle spacing modulo $[-\pi, \pi]$ and $\omega(k)$ is the dispersion relation of a linear chain: $\omega(k) = 2\left|\sin\frac{k}{2}\right|$. The above equations suggest that the underdamped sliding motion is dominated by resonance effects of the modes of the chain with the periodic potential: In the moving reference frame the modes with wave vector $|a|$ are excited by the potential with frequency v (3rd term on r.h.s.), the mode with wave vector $2a$ is excited by the term $\frac{b}{2}(x_a e^{ivt} + x_{3a} e^{-ivt})$ (4th term on r.h.s.) containing a frequency component $2v$. Generally, the mode with wave vector na is excited by a frequency nv leading to a resonance condition for the sliding velocity: $v \simeq v_n = \omega(na)/n$. This was already noted by Aubry and de Seze [9] and gives an explanation for the resonant velocities they observed in numerical simulations of the sliding motion. The above considerations apply to the commensurate and incommensurate case as well, note however that in the incommensurate case all modes are coupled to linear order in the way described above, since na ranges over all wave vectors of the chain. The resonances also dominate the behavior of the periodic solution of the equations of motion.

2.2. Periodic Solutions

Since for large damping the asymptotic solution is of the form (1), one can search for such solutions for arbitrary damping by inserting (1) in the equations of motion (2). This yields a differential-delay equation for the dynamic hull-function f_D:

$$\begin{aligned}v^2 f_D''(\xi) = &-\gamma v f_D'(\xi) \\ &- 2f_D(\xi) + f_D(\xi + a) + f_D(\xi - a) \\ &- b\sin(\xi + f_D(\xi)) + F - \gamma v \\ &\text{with } f_D(\xi) = f_D(\xi + 2\pi).\end{aligned} \tag{3}$$

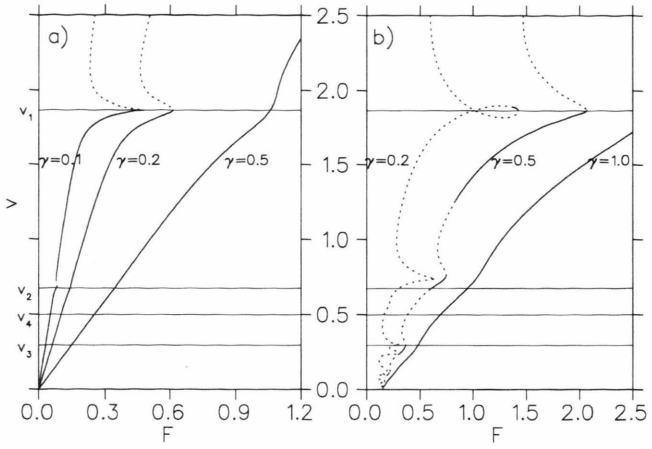

Fig. 1. Velocity-force characteristic of the periodic sliding state for different values of the potential strength b and the damping γ. Linear stable solutions are indicated by solid, and unstable solutions by dashed lines. The first four resonant velocities are indicated.
a) $b = 0.5$, γ =0.1, 0.2, and 0.5;
b) $b = 2.0$, γ =0.2, 0.5, and 1.0.

Due to the translational symmetry the solutions form one-parameter families because for a given solution $f_D(\xi)$, $f_D(\xi+\zeta)+\zeta$ is also a solution. One can thus impose the additional condition $f_0 = \int_0^{2\pi} f_D(\xi)d\xi = 0$. For a given velocity this states an eigenvalue problem for the force, having only a discrete set of solutions. In the overdamped limit there is only one solution. We solve (3) for the hull-function by Fourier transformation. The resulting algebraic equation

$$(v^2n^2 - \omega^2(na) - inv\gamma)f_n = bI_n(\{f_m\}) - (F - \gamma v)\delta_{n,0},$$

$$\text{where } f_n = \frac{1}{2\pi}\int_0^{2\pi} e^{-in\xi} f_D(\xi)d\xi$$

$$\text{and } I_n(\{f_m\}) = \frac{1}{2\pi}\int_0^{2\pi} e^{-in\xi}\sin(\xi + f_D(\xi))d\xi,$$

is solved numerically by truncating the set of equations at some order M. Alternatively one can solve a discrete version of (3) in real space, which gives the same results. Practically we obtain solutions for given values of the potential-strength and the damping by starting at a velocity greater than the highest resonant velocity and solving for the Fourier coefficients of f. This solution can be traced for decreasing values of the parameter v. In this way we are able do determine solutions as long as $v > O(M^{-1})$. At smaller velocities the solutions may become incorrect due to the truncation of the equations.

The linear stability of a given periodic solution is discussed using Floquet theory: Insertion of the Floquet Ansatz

$$\begin{pmatrix} x_j(t) \\ \dot{x}_j(t) \end{pmatrix} = e^{\beta t}\sum_{n=-\infty}^{\infty}\int_{-\pi}^{\pi} e^{i(kj+nvt)}\begin{pmatrix}\phi_k^n \\ \psi_k^n\end{pmatrix}dk$$

in the equations of motion, linearized along the periodic solution, leads to an eigenvalue problem for the Floquet exponents β:

$$\beta\phi_k^n = -inv\phi_k^n + \psi_k^n,$$

$$\beta\psi_k^n = -(\gamma + inv)\psi_k^n - \omega^2(k)\phi_k^n + \sum_m c_m\phi_{k-ma}^{n-m}$$

$$\text{with } c_n = -\frac{b}{2\pi}\int_0^{2\pi} e^{-in\xi}\cos(\xi + f_D(\xi))d\xi.$$

The eigenvalues of the truncated problem are calculated numerically and are used to estimate the stability of the periodic solution. The effect of the truncation is more severe in the stability analysis than in the calculation of the periodic solution itself, so that the estimates may be incorrect at small velocities.

Some results for different parameter values are presented in Figure 1: The first three resonant velocities can be identified in the $v(F)$ characteristic for $b = 0.5$. For $b = 2.0$ additional resonances appear with shifted resonant velocities. F approaches the static threshold force $F_c(b)$ for $v \to 0$.

As expected, solutions corresponding to negative-differential parts of the $v(F)$ characteristic are unstable. But the intervals of velocity values where the periodic solutions are unstable extend to higher values of the velocity than given by the negative-differential part of the characteristic. The instability of the solution in the positive-differential part of the characteristic is of Hopf type, i.e. the imaginary part of

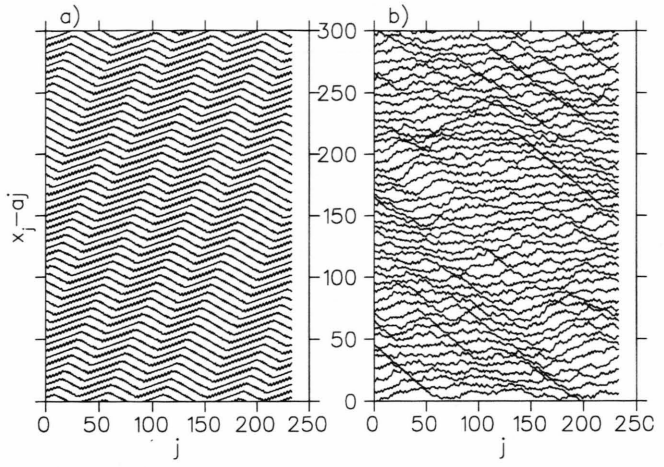

Fig. 2. Illustration of the sliding motion corresponding to the states marked by boxes in Figure 4. The position of the i-th particle minus i-times the mean particle spacing is plotted at times $t_n = n2\pi/v$.
a) $b = 2.0, \gamma = 0.5, F = 0.75$ and $v = 0.99$, quasiperiodic sliding;
b) $b = 2.0, \gamma = 0.1, F = 0.14$ and $v = 0.32$, spatio-temporal chaotic motion.

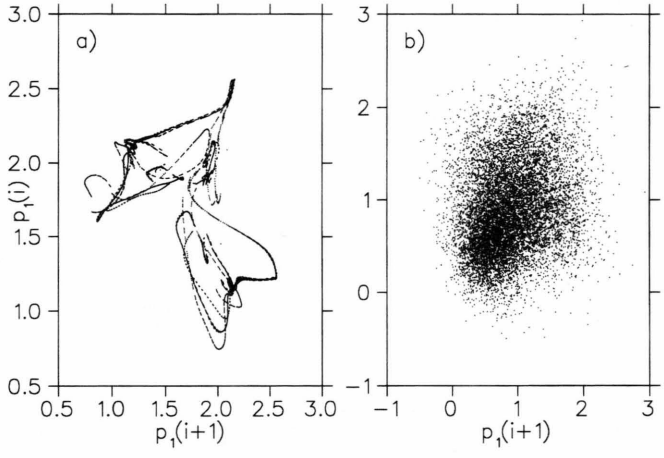

Fig. 3. Return map of the sliding motion for the states of Figure 2 a, b. The i-th maximum is plotted against the $i+1$-st maximum of the momentum of the first particle.

the Floquet exponent is non-zero. For a given potential strength the periodic solution loses its stability in an increasing range of velocity values for decreasing damping.

2.3. Numerical Simulations

As stated above the periodic sliding solutions are unstable for small values of the damping and one expects more complex sliding behavior. This is investigated by direct numerical integration of the equations of motion (2) for a system of $N = 233$ particles with $L = 377$ (the simulations were done with a variant of the Verlet algorithm and checked against with a fourth-order Runge-Kutta method).

We first mention that numerically calculated and simulated periodic motions are in good agreement. The predicted instability of the periodic solution is observed. The observation of motions which are quasiperiodic or of higher periodicity is consistent with the fact that the instability of the periodic solution can occur with arbitrary imaginary part of the Floquet exponent. For lower values of the damping spatio-temporal chaotic solutions are found (Figures 2 and 3). In the parameter regime with quasiperiodic or chaotic solutions multistability of attractors is common. Different sliding states are found for the same value of the force, especially for sliding states with velocities near a resonant velocity v_n. This leads to hysteresis effects when increasing and decreasing the force and measuring the mean velocity (Figure 4). The depinning transition is also found to be subcritical for small enough damping.

3. Conclusion

We have discussed the periodic sliding motion of the underdamped dynamics of the Frenkel-Kontorova model, which was seen to be dominated by resonances. This type of resonances is also found in the

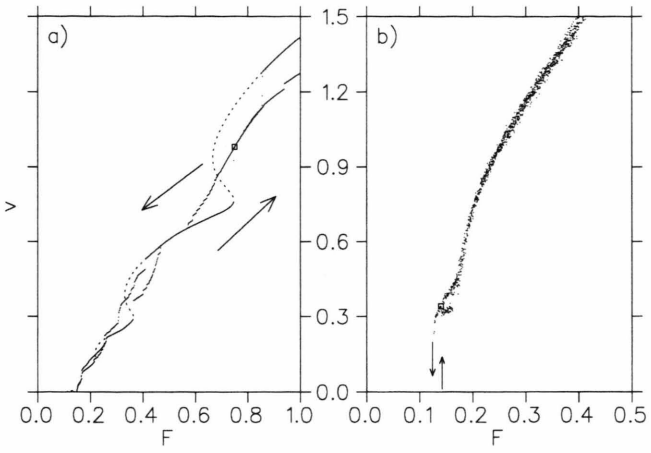

Fig. 4. Velocity-force characteristic obtained by increasing and decreasing the force stepwise and relaxing the system to an attractor.
a) $b = 2.0, \gamma = 0.5$ The dashed line corresponds to the unstable periodic motion. Solid lines correspond to periodic or quasiperiodic motion;
b) $b = 2.0, \gamma = 0.1$ Hysteretic depinning occurs.

behavior of small Josephson junction arrays [5], and our discussion of the stability of the periodic motion suggests that in larger arrays nonperiodic motions may occur. Thus it will be interesting to discuss the periodic motion and its stability of commensurate systems, especially in dependence on the order of commensurability and the number of particles of the system.

In modeling the dynamics of CDW systems the quenched randomness of the pinning centers has to be taken into account, so that the resonance effects will be of a different type in these systems. Nevertheless there is experimental evidence that the motion of some CDW systems shows more complex behavior, for example hysteretic depinning [4], which can not be described by overdamped models with one-dimensional order parameter. But it is not clear if these observations are due to inertia effects. In this context the complex sliding motion in the inertia dominated dynamics of the chain, especially in the large particle limit, is subject to further investigation.

If the model is considered as a simple friction system, the behavior at small velocities is of interest, and since the resonant velocities are dense for $v \to 0$, this limit is not trivial. The sliding motion of the incommensurate chain in the limit of small damping, i.e. $\gamma \to 0$, also deserves further investigation.

Acknowledgements

I thank F. J. Elmer for a critical reading of the manuscript and M. Bünner for interesting communication on the CDW subject. This work was supported by the Swiss National Science Foundation.

[1] T. A. Kontorova and Ya. I. Frenkel', Zh. Eksp. Teor. Fiz. **8,** 1340, (1938).
[2] F.-J. Elmer, Phys. Rev. E **50,** 4470, (1994).
[3] G. M. McClelland, Friction at Weakly Interacting Interfaces, in Springer Series in Surface Science Vol.17, ed. M. Grunze and H. J. Kreuzer (1989), p. 1.
[4] P. B. Littlewood, Computer Simulations of CDW Dynamics, in Charge Density Waves in Solids, ed. L. P. Gor'kov and G. Grüner (1989), p. 321.
[5] H. S. J. van der Zant et al., Phys. Rev. Lett. **74,** 174, (1995).
[6] S. Aubry, in Solitons and Condensed Matter, Solid State Sciences Vol. 8, ed. A. Bishop and T. Schneider (1978), p. 264,
M. Peyrard and S. Aubry, J. Phys. C **16,** 1593 (1983).
[7] S. N. Coppersmith and D. S. Fisher, Phys. Rev. B **38,** 6338, (1988).
[8] A. A. Middleton, Phys. Rev. Lett. **68,** 670, (1992).
[9] S. Aubry and L. de Seze, in Festkörperprobleme XXV (1985), p. 59.